Membrane Technology
ISSN (online): 1873-4049

Machine Vision-Based Straightness Measurement of Pressed Joints

Tianhang Jiang [1], Yong He [1], Hanjie Yuan [1], Liang Chen [1], Haiao Tan[1], Longjie Wu[1], Ziming Liu[2,*]

[1]*Guangdong Power Grid Co., Ltd. Zhaoqing Power Supply Bureau, Zhaoqing, 526000, China*
[2] *Guangzhou Saihaoda Intelligent Technology Co., Ltd, Guangzhou, 510000, China*
** Corresponding Author.*

Abstract:
To address the issues of complexity, time consumption, and low detection accuracy in traditional straightness detection methods for pressed joints, a non-contact measurement method based on machine vision is proposed. The main approach is to rotate the joint and acquire images at different angles. Bilateral filtering is used to denoise the images. Considering the potential reflections and simple background of the joint, color space conversion and local binary patterns are introduced to capture local texture features. Through feature stitching and principal component analysis to adapt the Grab Cut algorithm, the joint region is segmented. The weighted average method is used to grayscale the extracted image, and after Canny edge detection, edge connection, and filling algorithm, the edge contour image of the joint is obtained. According to the contour information and the straightness measurement method proposed in this paper, the center coordinates of each cross-section of the joint are obtained, and then the least squares method is used to evaluate the straightness error of the joint to judge the bending condition of the joint. Finally, comparative experiments show that the detection system has high detection accuracy and reliable detection results.

Keywords: Machine vision, straightness error, Grab Cut algorithm, straightness evaluation.

INTRODUCTION

In overhead transmission lines, the straightness detection of pressed joints [1,2] is one of the key indicators for evaluating the pressing quality. If the straightness of the pressed joint does not meet the standard, it may lead to poor contact, reduced mechanical strength, and other problems, thus affecting the stability of the electrical connection, increasing the risk of breakage, reducing the efficiency of power transmission, threatening the safety of the transmission line, and leading to higher maintenance and inspection costs. Therefore, it is crucial to ensure that the straightness of the pressed joint is qualified.

In terms of straightness detection, Reference [3] proposes a track straightness detection method based on dual laser sensors. This method utilizes two laser sensors installed at different positions to measure the laser reflection data at various positions on the track surface, and then calculates the straightness error of the track. Reference [4] employs a high-precision laser profilometer to measure the straightness of steel rails from four directions. By establishing a mathematical model based on the external boundary support points, the straightness error is finally calculated using the least squares method. Reference [5] presents an online dimensional detection technology for conical workpieces with a half-cone angle of 45° based on machine vision. This method can achieve real-time measurement of the workpiece's straightness and roundness. Reference [6] explores an improved Wollaston prism sensing heterodyne interferometer, which can simultaneously measure the straightness error and its position. Reference [7] proposes an innovative straightness measurement method for low-temperature valves. By arranging high-precision sensors at key positions inside the valve to collect the offset data of the internal structure, a mathematical model of the signal propagation path and straightness error is constructed, and the actual straightness of the valve is calculated using an inversion algorithm. Reference [8] obtains the straightness error of a slender shaft by segmentally acquiring images and codes of the shaft and reference objects, extracting the feature point coordinates of the reference objects, and combining the coding information to establish a mathematical model of the diameter, center coordinates, and external parameters.

The straightness measurement object of this paper is a pressed joint similar to the combination of a hexagonal shaft and a cylinder. The laser sensor-based straightness measurement methods in References [3] [4] are more suitable for objects with planar structures such as steel rails. The method in Reference [5] is targeted at conical workpieces with a half-cone angle of 45° and is not applicable to the research object of this paper. The methods in other references also have specific limitations or high costs. Therefore, this paper proposes a machine vision-based measurement method for pressed joints, which has high detection efficiency and accuracy, as well as real-time performance and data recording capabilities. This method utilizes a calibrated CCD camera to acquire images of the joint, and after image filtering, the improved Grab Cut algorithm is used to segment the joint image. By performing edge detection on the preprocessed image, the geometric contour information of the joint is obtained. Finally, the straightness of the joint is detected through the straightness error measurement method proposed in this paper.

COMPOSITION OF THE STRAIGHTNESS MEASUREMENT SYSTEM

System Composition

The composition of the pressed joint straightness measurement system is shown in Figure 1. The system mainly consists of a linear electric displacement platform, a rotary electric platform, a fixture, a CCD camera, a motion control card, and a computer.

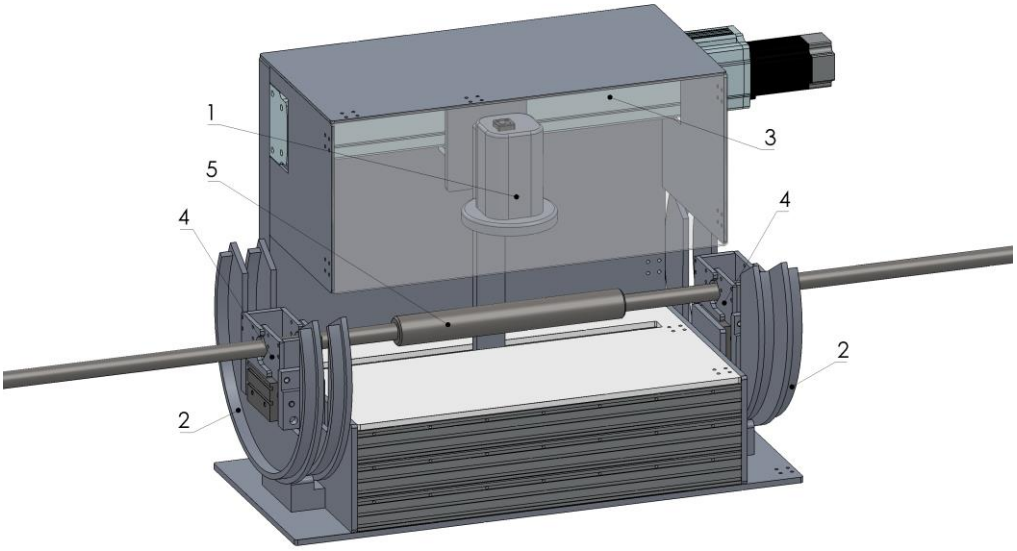

1. CCD camera 2. Rotating electric module 3. Linear motion module 4. Fixture 5.Joint

Figure 1. Structure diagram of the straightness measurement system

Measurement Method

The straightness error of a pressed joint is the straightness error of the line connecting the centers of each cross-section of the actual joint. In order to accurately measure the straightness error of the axis of the pressed joint after pressing, it is necessary to collect the edge contour information of the joint. After calibrating the camera, the joint is placed horizontally on the workbench, and the linear electric displacement platform is controlled to adjust the camera to a suitable position. The initial position is 0°, and the rotary electric platform is controlled to rotate. The camera simultaneously acquires images of the joint when the rotary electric platform rotates 0°, 90°, and 180°, and the acquired images are stored in the computer. Image processing algorithms are used to preprocess the stored images, and foreground segmentation is performed. After grayscale processing, edge detection is performed. After extracting the edge contour information of the joint, the axis of the joint to be measured is fitted, and finally, the straightness error is calculated according to the evaluation method. The measurement method flowchart is shown in Figure 2.

JOINT CONTOUR EXTRACTION AND STRAIGHTNESS MEASUREMENT

Edge Contour Extraction

The measurement method of the straightness error of the pressed joint in this paper depends on the edge contour information of the pressed joint. The geometric contour of the joint, as a key parameter, directly affects the accuracy and reliability of the straightness measurement results. In the field of image edge detection, compared with traditional edge detection algorithms, the Canny algorithm [9] performs better in suppressing noise and preserving edges, but there are still shortcomings in preserving edge details and reducing false edges. Therefore, this paper first uses the improved Grab Cut algorithm [10] to segment the image and extract the main body of the joint. By doing so, more edge information can be preserved when performing edge detection.

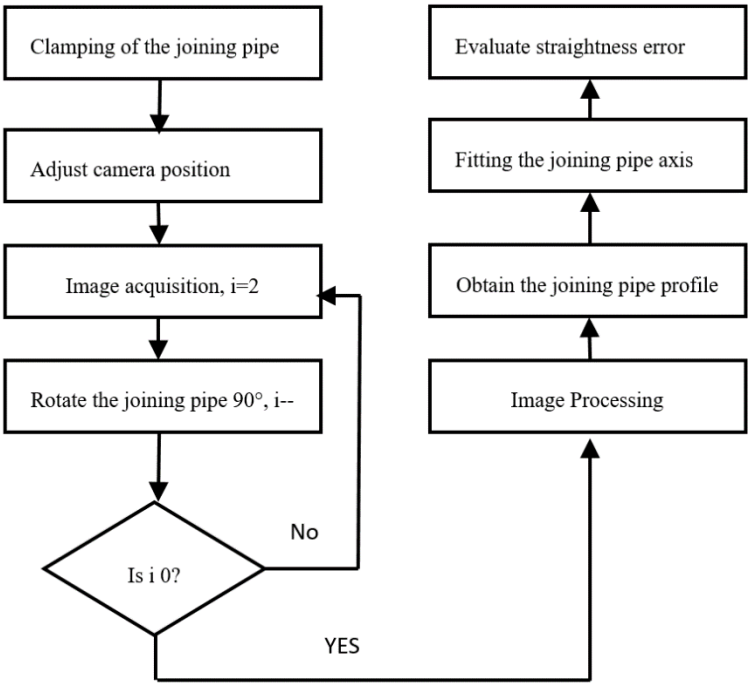

Figure 2. Flowchart of straightness error measurement

Camera calibration

Since the straightness error needs to be measured, the camera needs to be calibrated first. In this paper, MATLAB is used for camera calibration [11]. A calibration board (checkerboard pattern) is prepared and multiple sets of images containing the calibration board are captured. Then, using the Camera Calibrator tool provided by MATLAB, the calibration board images are imported and the corner point information of the calibration board is extracted. The software calculates the intrinsic parameters (such as focal length, principal point, distortion coefficient) and extrinsic parameters (the pose of the camera relative to the calibration board) of the camera through the fitting of the spatial coordinates and image coordinates of the corner points. At the same time, the calibration board is placed parallel to the imaging plane of the camera and coincident with the axis of the rotary electric platform, and its image is acquired. By comparing the actual size of the calibration board at this time with the image coordinates, the pixel equivalent (the actual physical size corresponding to each pixel) can be further obtained. Accurate camera calibration can improve the reliability and accuracy of subsequent measurements.

Image filtering

During the image acquisition process, it is inevitable to be disturbed by some factors, which are also called noise. Noise can hide the details and features in the image and affect some important edge information. For the Grab Cut algorithm used for foreground and background segmentation, the accuracy of the image edge is crucial. Using a suitable filtering method can help keep the boundary between the foreground and background clear. Bilateral filtering [12] is a non-linear filtering technique. Unlike ordinary Gaussian filtering [13], bilateral filtering also considers the similarity of pixel values (color information) and spatial distance during smoothing, so it can effectively preserve edge details in the image and prevent excessive blurring. The filtering function formula is as follows:

Spatial kernel:

$$d(x, y, k, l) = \exp\left(-\frac{(x-k)^2+(y-l)^2}{2\sigma_d^2}\right) \quad (1)$$

Range kernel:

$$r(x, y, k, l) = \exp\left(-\frac{|f(x,y)-f(k,l)|^2}{2\sigma_r^2}\right) \quad (2)$$

Weight coefficient:

$$w(x, y, k, l) = d(x, y, k, l) \times r(x, y, k, l) \quad (3)$$

Bilateral filtering function expression:

$$g(k,l) = \frac{\sum_k^l f(x,y)w(x,y,k,l)}{\sum_k^l w(x,y,k,l)} \quad (4)$$

Improved Grab Cut for Joint Region Segmentation

Acquired images of the pressed joint may contain noise, shadows, and reflections, which can affect the accuracy of subsequent edge detection. By separating the joint region from other irrelevant backgrounds, the influence of interference on the straightness error measurement can be effectively reduced.

The Grab Cut algorithm is an interactive image segmentation method based on graph theory, used to extract foreground regions from complex backgrounds. The Grab Cut algorithm treats an image as an unweighted undirected graph, where each node represents a pixel in the image, and each node is connected to surrounding nodes with a weight. The weight value is used to measure the similarity between pixels. There are two types of edges in the graph: t-link and n-link. The former is the link between a pixel and the foreground or background, representing the possibility that the pixel belongs to the foreground or background. The latter represents the connection between pixels, used to maintain local consistency of the image and ensure that adjacent pixels with similar colors or intensities are classified into the same category as much as possible. The Grab Cut algorithm is based on the graph cut technique [14], which finds an optimal segmentation method through the graph cut algorithm to minimize the energy cost between the foreground and background.

The Grab Cut algorithm uses a Gaussian mixture model (GMM) [15] in the RGB color space to statistically model the color distribution of the foreground and background. The user marks the foreground and background regions with simple annotations, and the algorithm uses the maximum a posteriori probability (MAP) [16] estimate to continuously optimize the segmentation results. The Grab Cut algorithm uses an energy function to represent the segmentation quality of the image. The energy formula for the entire image is as follows:

$$E(a,k,\theta,z) = U(a,k,\theta,z) + V(a,z) \quad (5)$$

Where: U is the regional term; V is the smoothness term. The GMM label of each pixel in the original image is denoted by k = (k1, ..., kn, ..., kN), where kn = (1, 2, ..., K). The regional term quantifies the degree of match between the color of each pixel in the image and the foreground and background models, and the smoothness term reflects the label consistency between adjacent pixels. The regional term is defined as follows:

$$U(a,k,\theta,z) = \sum_n D(a_n,k_n,\theta,z_n) \quad (6)$$

Where: D is the data term, which assigns a cost to each pixel, representing the possibility that it belongs to the foreground or background. This possibility is measured by the negative log probability, defined as shown in equation (7).

$$D(a_n,k_n,\theta,z_n) = -\log\pi(a_n,k_n) + \frac{1}{2}\log\det\Sigma(a_n,k_n)$$
$$+\frac{1}{2}[z_n-\mu(a_n,k_n)]^T\Sigma(a_n,k_n)^{-1}[z_n-\mu(a_n,k_n)] \quad (7)$$

Where θ is the model parameter of GMM, and through the above transformation, θ can be expressed as:

$$\theta = \{\pi(a,k),\mu(a,k),\Sigma(a,k),a=0,1,k=1,2,\cdots,K\} \quad (8)$$

Where: π is the weight coefficient of the Gaussian component k; μ is the mean vector of the Gaussian component k; Σ is the covariance matrix of the Gaussian component k; and k is the index of the component in the Gaussian mixture model.

In the RGB space, the smoothness term V uses Euclidean distance [17] (two-norm) to measure the similarity between two elements. The greater the difference between two neighboring elements, the smaller the energy. The calculation method is as follows:

$$V(a,z) = \sum_{\substack{(m,n)\in C \\ a_n\neq a_m}} \exp\left(-\beta\|z_m - z_n\|^2\right) \quad (9)$$

The Grab Cut algorithm iteratively updates model parameters and re-classifies pixels to optimize the energy function, resulting in the convergence and minimization of the energy function. This process yields the boundary nodes for segmenting the foreground and background of the image, thereby segmenting the foreground and background regions of the original image. The result of Grab Cut segmentation of the joint is shown in Figure 3a. It can be observed that part of the background in the green

rectangular box is judged as the foreground object, and the segmentation effect is poor.

The images collected in this paper have a simple background, and the joint is a metal part, which has a reflective problem under illumination and may cause a complex distribution of color features. The foreground region is easily misjudged as the background. To address this, this paper improves the Grab Cut segmentation process. First, the RGB color space of the original image is converted to the HSV color space. In reflective scenes, the brightness information in the V channel is often biased high, while the hue H is used to distinguish color attributes. When the background is simple, it is very stable, and the saturation S has a small impact on the reflective area. Furthermore, local binary patterns (LBP) [18] features are introduced. Reflection causes large changes in color, but the texture characteristics of metals are relatively stable. LBP, as a texture descriptor, can capture the texture features of local regions and compensate for the shortcomings of color features. The LBP features of the grayscale channel of the input image are calculated, and a texture feature map is generated using the classic LBP operator. The LBP features are concatenated with the features of the HSV color space to form a multi-modal feature vector. The four-channel feature image is converted into a three-channel image through principal component analysis (PCA) [19] for subsequent modeling, making it adaptable to the Grab Cut algorithm. Finally, the Grab Cut algorithm is used to segment the joint region based on the preprocessed image, and the results are compared with the traditional Grab Cut algorithm, as shown in Figure 3b. It can be seen that the joint is completely segmented from the background, and the segmentation effect is better.

The improved Grab Cut algorithm has higher robustness and accuracy, can achieve better segmentation results, and retain richer edge contour information, further improving the accuracy of subsequent edge detection.

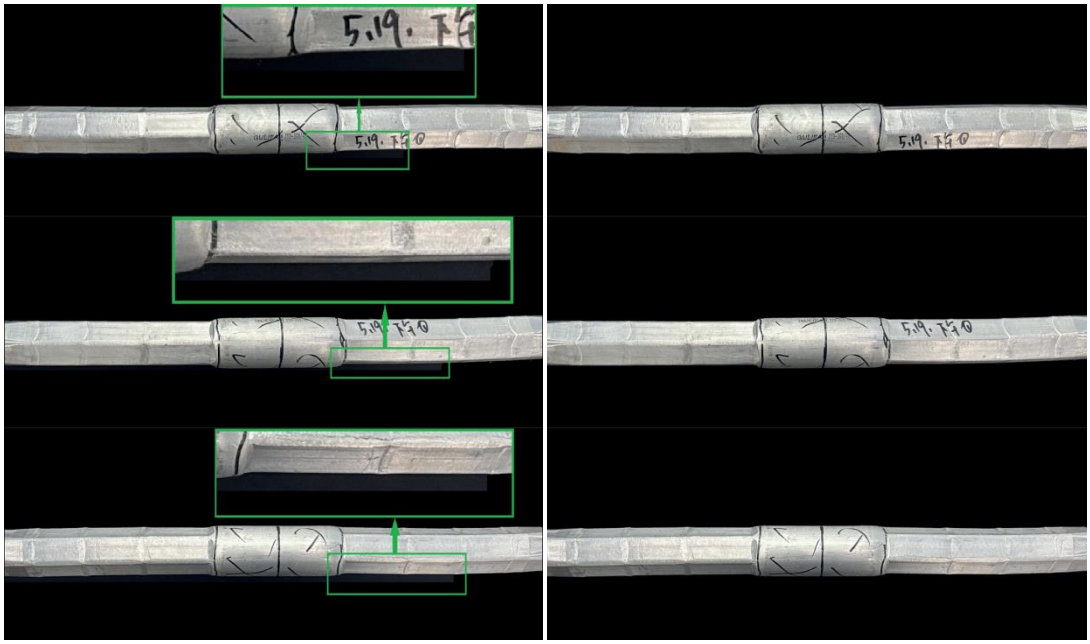

a) Grab Cut joint segmentation image b) Improved Grab Cut joint segmentation image

Figure 3. Grab Cut segmentation effects before and after optimization

Edge detection

For the images with the foreground extracted by the Grab Cut algorithm, we only care about the edge information. The redundant color information will increase the computational complexity and processing time during edge detection. Therefore, the extracted joint image is converted into a grayscale image. For the straightness error detection of the joint, preserving the completeness and accuracy of the contour is crucial for the subsequent fitting of the joint axis. Grayscale conversion transforms a color image into a grayscale image, thereby simplifying the image matrix and reducing the computational complexity. At the same time, it retains the gradient information between pixels, which is convenient for subsequent Canny edge detection. In this paper, the weighted average method is used to convert the joint image into grayscale, where the weight coefficients of RGB are obtained based on the human eye's sensitivity to different color components. The calculation formula is as follows:

$$\text{Gray} = 0.299\text{R} + 0.587\text{G} + 0.144\text{B} \tag{10}$$

where: Gray is the grayscale value of the pixel in the grayscale image; R, G, and B are the values of the red, green, and blue

channels of the original image, respectively.

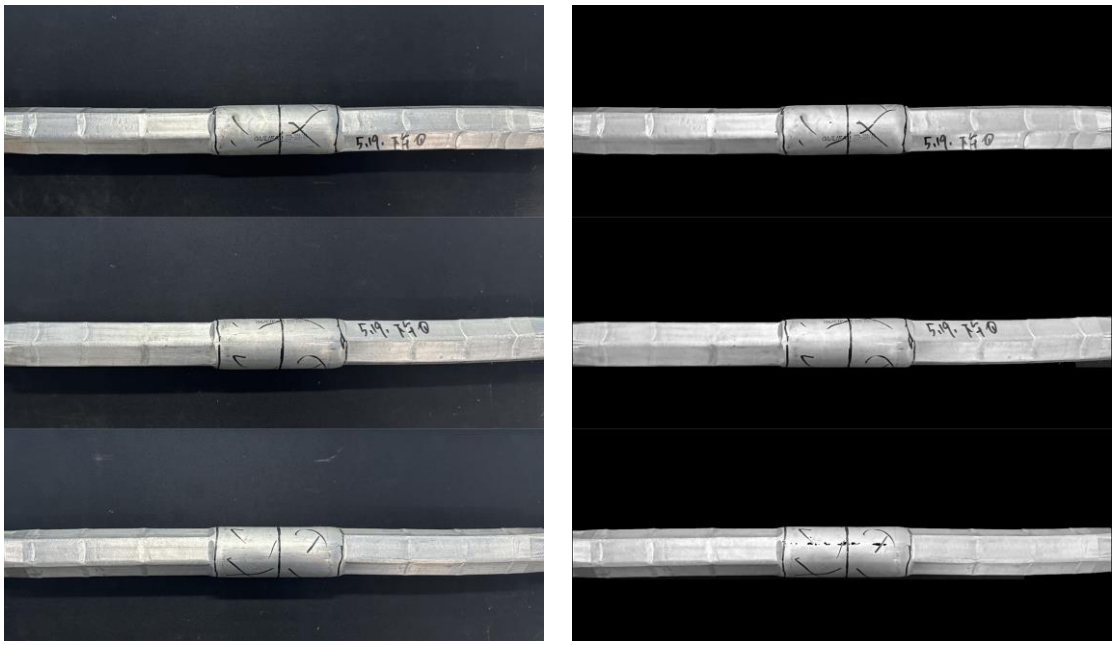

) Joint images at 0°, 90°, and 180° b) Grayscale image of the joint

Figure 4. Grayscale images of the joint after grayscale processing

The method for measuring the straightness error of the joint studied in this paper relies on the edge contour information of the joint. Its geometric contour, as a key parameter, and the accuracy and completeness of the contour are crucial to the measurement results.

The basic idea of edge detection is to detect the boundary contour of an object by identifying areas with significant changes in image grayscale values. The gradient of the image can be calculated to detect edges. In this paper, the Canny algorithm is used for edge detection. The Canny algorithm calculates the gradient magnitude and direction of the smoothed image using the Sobel operator. Each pixel is checked to see if it is a local maximum along the gradient direction. Then, non-maximum suppression is performed to remove non-edge pixels. Further, a double-threshold strategy is used to classify edges, where the high threshold determines strong edges and the low threshold determines weak edges. By connecting edges, weak edges are connected to strong edges, and isolated weak edges are removed, resulting in a clear and continuous edge image. By connecting the edge image, the edge contour curve of the joint is obtained. Figure 5 shows the edge detection images of a joint at three angles.

Straightness Measurement Method

straightness tolerance introduction

The joint studied in this paper is an axially symmetric object, and its axial straightness error is used as the evaluation standard. This belongs to the straightness error in any spatial direction, that is, in any direction, the actual straightness feature is not constrained by a specific direction. The straightness tolerance zone is defined as a cylindrical region with a diameter of t, as shown in Figure 6. It is generally used for error evaluation of shaft-like parts or precision guides.

Measurement method

To detect the spatial straightness error of the joint, this paper rotates the joint to obtain its two-dimensional projection images at 0°, 90°, and 180° rotation angles, respectively. Thus, the two-dimensional projection coordinates of the joint axis in the image are obtained. Due to the straightness error of the joint, the position of the joint axis changes with the rotation of the joint. The spatial coordinates of the joint are obtained by calculating the change in the coordinates of the axis.

Within the joint region of the image after edge detection, N measurement points are selected at equal intervals, and the spatial coordinates of the centers of each cross-section are calculated at these selected measurement points.

Due to the possible tilt angle or straightness error of the joint image during acquisition, the upper and lower edge points may be distributed asymmetrically, causing a large error in the central axis. To reduce this error, this paper adopts a local region search

and comparison method. When the coordinate point of the measurement position is closest to the pixel point of the upper edge, the midpoint of these two points is taken as the center point of the cross-section, as shown in Figure 7.

) Joint images at 0°, 90°, and 180° b) Edge image of the joint

Figure 5. Edge contour of the joint

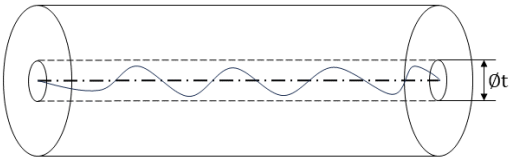

Figure 6. Any direction

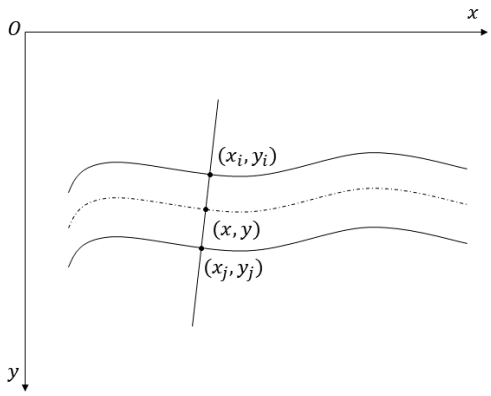

Fig. 7. Schematic diagram of the calculation of the pixel coordinates of the central axis

The expression is as follows:

$$\sqrt{(y_i - y_j)^2 + (x_i - x_j)^2} = \min\{H\} \tag{11}$$

$$\begin{cases} x = \frac{x_i + y_j}{2} \\ y = \frac{y_i + y_j}{2} \end{cases} \tag{12}$$

To reduce the calculation time, this paper selects the upper edge point (x_i, y_j) corresponding to the horizontal coordinate of the lower edge point and 3 points in the left and right neighborhoods, a total of 7 points, and calculates the distances between these points and the lower edge point, respectively. According to the above formula, the corresponding geometric coordinates of the joint axis are obtained.

To solve the spatial straightness of the joint, it is necessary to calculate the three-dimensional coordinates of the center of the cross-section corresponding to the measurement position. The axis direction of the rotation axis is set as the Z-axis, and the coordinate system of the cross-section corresponding to the measurement point is established (as shown in Figure 8). Assuming that the center of the cross-section at a certain measurement position is (x, y, z_k) before rotation, and its pixel coordinate in the image is (u, v_1), where k represents the order of the measurement point (k =0, 1, 2, ... N). When the cross-section rotates 90 degrees, the coordinates of its center become(x_1, y_1), and the corresponding pixel position in the image is (u, v_2); when the part rotates to 180 degrees, the coordinates of the center of the cross-section become (x_2, y_2), and the corresponding position in the image is (u, v_3). At this time, the relationship between the spatial coordinates is:

$$\begin{cases} x_1 - x = G \cdot (v_2 - v_1) \\ x_2 - x_1 = G \cdot (v_3 - v_2) \end{cases} \tag{13}$$

Where G is the pixel equivalent, obtained by camera calibration. By combining the above two equations, the spatial coordinates of the center of the cross-section corresponding to a certain measurement point of the joint at the initial position can be obtained. The spatial coordinates of other measurement points can be obtained in the same way.

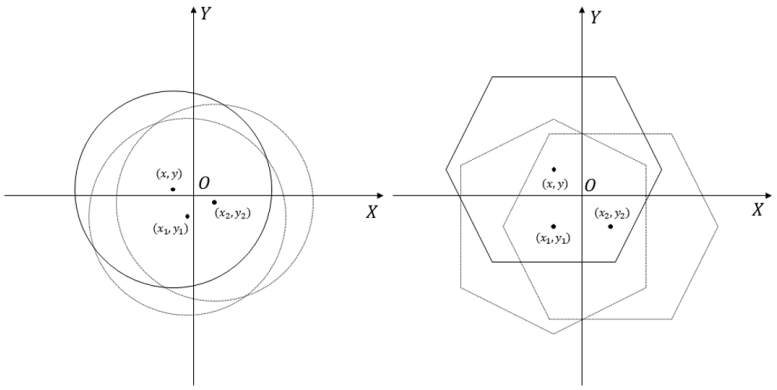

a) Cross-section is a circle b) Cross-section is a regular hexagon

Fig. 8. Schematic diagram of the change in the center of the cross-section

Evaluation method

After obtaining the spatial coordinates of the centers of each cross-section of the joint according to the straightness error measurement scheme, the least squares method [20] is used to fit the evaluation line. This method is suitable for processing a large amount of measurement data and can minimize the error between all measurement points and the fitted straight line through optimization of the fitting process. At the same time, it can reduce the influence of individual outliers on the evaluation results, making the evaluation results more stable and reliable.

Through the above calculation, the three-dimensional coordinates $O_i(x_i, y_i, z_i)$ of the centers of each cross-section of the joint are obtained. The least squares method is used to fit a straight-line equation for each center point. The fitted straight line is taken as the evaluation baseline l_s. By comparing the shortest distance di from each cross-section center point to the evaluation baseline l_s, the maximum distance d_{max} in d_i is obtained. Then, the region enclosed by the cylindrical surface with l_s as the axis and the maximum value d_{max} as the radius is the straightness error region of the joint, and the error value is the diameter D of the cylindrical surface, which is $2d_{max}$. The principle of this evaluation method is shown in Figure 9:

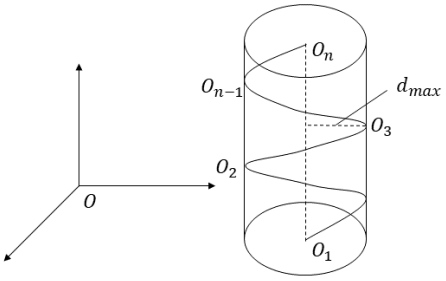

Figure 9. Schematic diagram of the least squares evaluation principle

The specific calculation process is as follows:

Let the coordinates of the center of each cross-section of the part be $O_0(x_0, y_0, z_0)$ (i = 0, 1, 2...N), and a, b, c be the unit direction vectors of the evaluation baseline ls. In order to simplify the calculation and make the error distribution more uniform, the arithmetic mean point $O_0(x_0, y_0, z_0)$ of all points is taken as a point on the evaluation baseline, which can improve the stability of the fitting process.

The evaluation baseline can be obtained as follows:

$$\frac{x-x_0}{a} = \frac{y-y_0}{b} = \frac{z-z_0}{c} \tag{14}$$

Where the unit direction vector:

$$a^2 + b^2 + c^2 = 1 \tag{15}$$

The arithmetic mean point $O_i(x_i, y_i, z_i)$ can be expressed as:

$$\begin{cases} x_0 = \frac{1}{n}\sum_{i=1}^{n} x_i \\ y_0 = \frac{1}{n}\sum_{i=1}^{n} y_i \\ z_0 = \frac{1}{n}\sum_{i=1}^{n} z_i \end{cases} \tag{16}$$

Calculate the distance d_i from each cross-section center to the evaluation baseline l_s:

$$d_i = \sqrt{\frac{\begin{matrix}[b(x_i-x_0)-a(y_i-y_0)]^2+ \\ [c(x_i-x_0)-a(z_i-z_0)]^2+ \\ [c(y_i-y_0)-b(z_i-z_0)]^2\end{matrix}}{a^2+b^2+c^2}} \tag{17}$$

According to the principle of the least squares method, the sum of the squares of the distance d_i must be minimized. Let:

$$E = \sum_{i=1}^{n} d_i^2 \tag{18}$$

Taking partial derivatives with respect to a, b, and c, we have:

$$\frac{\partial E}{\partial a} = \frac{\partial E}{\partial b} = \frac{\partial E}{\partial c} = 0 \tag{19}$$

From the above equations, the baseline direction vector can be obtained:

$$\begin{cases} a = \frac{b\sum_{i=1}^{n}(x_i-x_0)(y_i-y_0)+c\sum_{i=1}^{n}(x_i-x_0)(z_i-z_0)}{\sum^{i=1n}(y_i-y_0)^2+\sum^{i=1n}(z_i-z_0)^2} \\ b = \frac{a\sum_{i=1}^{n}(y_i-y_0)(x_i-x_0)+c\sum_{i=1}^{n}(y_i-y_0)(z_i-z_0)}{\sum_{i=1}^{n}(x_i-x_0)^2+\sum_{i=1}^{n}(z_i-z_0)^2} \\ c = \frac{a\sum_{i=1}^{n}(z_i-z_0)(x_i-x_0)+b\sum_{i=1}^{n}(z_i-z_0)(y_i-y_0)}{\sum_{i=1}^{n}(x_i-x_0)^2+\sum_{i=1}^{n}(y_i-y_0)^2} \end{cases} \tag{20}$$

From the above calculation process, the straight-line equation of the baseline l_s can be obtained. At the same time, according to formula (18), the shortest distance d_i between each measurement point and the baseline can be obtained. By searching and comparing, the maximum value d_{max} is found, and then the spatial straightness error f of the joint is:

$$f = D = d_{max} \tag{21}$$

STRAIGHTNESS EVALUATION RESULTS

After the joint is crimped, it is stipulated that the straightness error of the joint shall not exceed 2% of the tube length. In order to verify the accuracy of the straightness measurement method in this paper, two crimped joints were selected for multiple measurement experiments according to the straightness detection algorithm of this paper. The parameters of the crimped joints 1 and 2 are both 33.588 mm for the opposite edge distance, 40 mm for the diameter of the uncrimped cylindrical region, and 490 mm for the total length.

A coordinate measuring machine, SIRIUS CROMA PLUS 686 05.06.04, was used to measure the straightness error of joints 1 and 2 under standard environmental conditions. The probe configuration of the coordinate measuring machine is standard force, probe length is 10 mm, and probe tip diameter is 4 mm. The specific parameters are shown in Table 1.

Table 1. Parameters of SIRIUS CROMA PLUS 68605.06.04

MPE(μm)		Travel Range (mm)			Dimensions (mm)			Maximum weight of measured workpiece (kg)	Machine weight (kg)
MPEE	MPEP	X	Y	Z	Lx	Ly	Lz		
2.3+L/300	2.5	600	800	600	1150	1735	2630	300	730

In the table: MPEE is the maximum permissible error of length measurement; MPEP is the maximum permissible probing error; L is the measurement length.

After the coordinate measuring machine measured the straightness of the two joints multiple times and took the average, the straightness error of joint 1 was 7.793 mm, and the straightness error of joint 2 was 10.681 mm. Joint 1 meets the crimping requirements, while joint 2 does not meet the crimping requirements.

The straightness of joints 1 and 2 was measured using the method in this paper, with N = 10, step length L = 50 mm, and repeated measurements 3 times. The acquired images and some of the processed images of joint 1 are shown in Figure 10. The detection results of joint 1 are shown in Table 2, where d_i is the distance from each sampling point to the least squares evaluation baseline, and the deviation of the joint axis is shown in Figure 11.

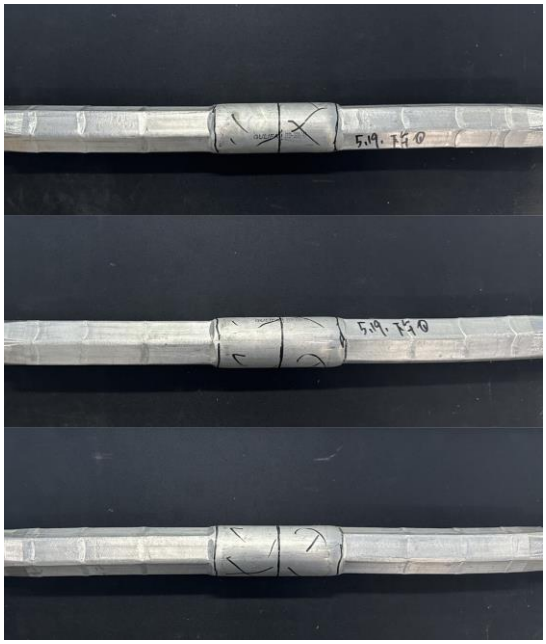

a) Images at 0°, 90°, and 180°

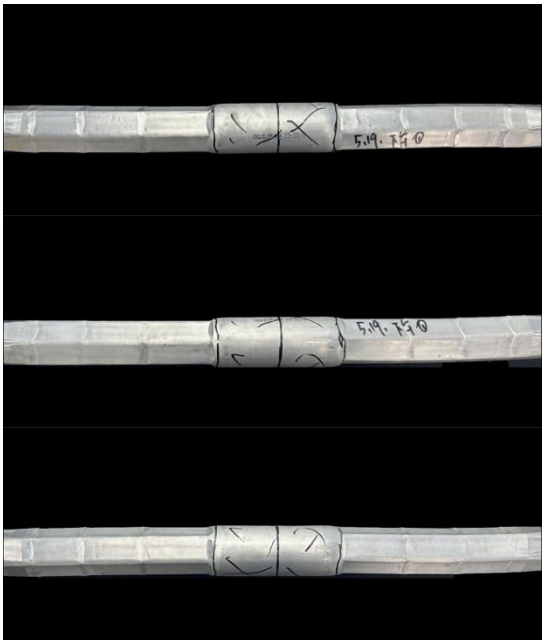

b) Grab Cut joint segmentation image

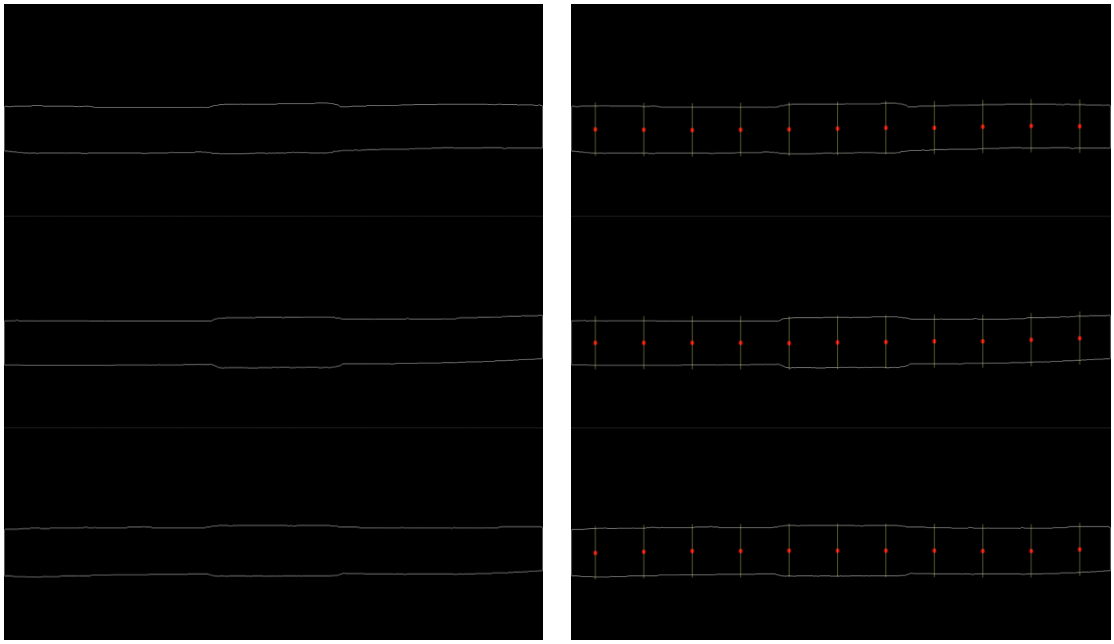

c) Joint edge image d) Joint sampling point image

Figure 10. Processed image of joint 1

Table 2. Experimental data of joint 1 (mm)

Sampling Location	d_i		
	First Sampling	Second Sampling	Third Sampling
20	3.239	3.075	3.322
70	3.679	3.349	3.865
120	3.020	3.157	3.075
170	2.391	2.358	2.228
220	2.504	2.389	2.261
270	2.928	3.537	2.898
320	3.847	3.679	3.959
370	3.624	3.349	3.708
420	2.285	2.526	2.635
470	4.061	4.093	3.807
d_{max}	4.061	4.093	3.959
Straightness error	8.122	8.186	7.918
Mean straightness error	8.075		

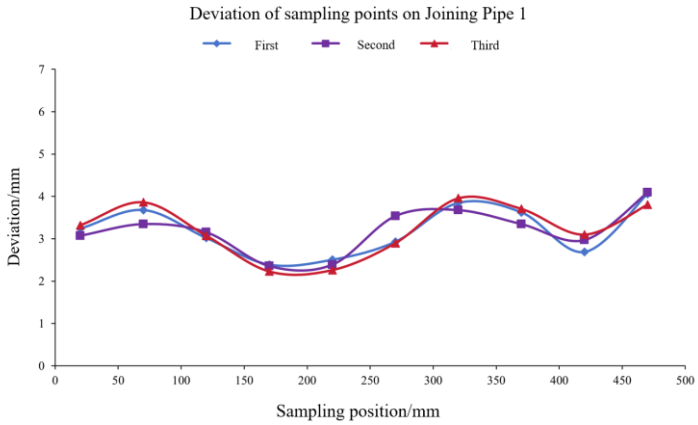

Figure 11. Axial deviation of joint 1

The acquired images and some of the processed images of joint 2 are shown in Figure 12. The detection results of joint 2 are shown in Table 3, and the axial deviation of the joint is shown in Figure 13.

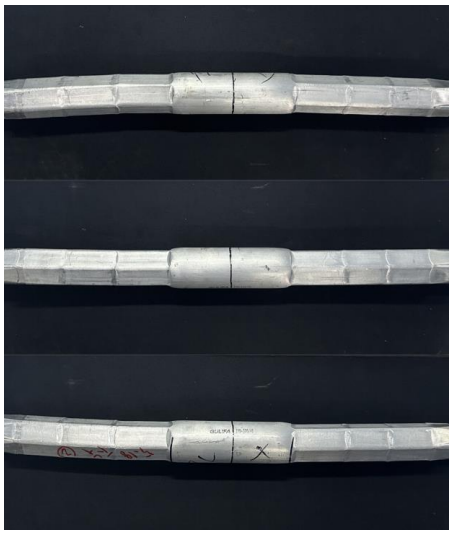

a) Images at 0°, 90°, and 180°

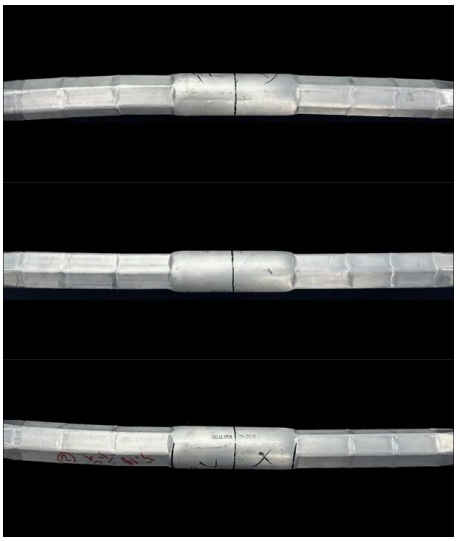

b) Grab Cut joint segmentation image

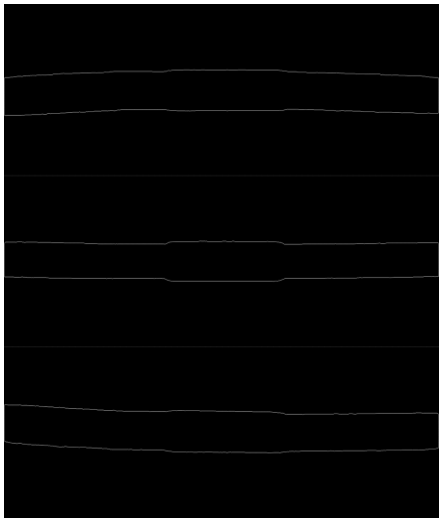

c) Joint edge image

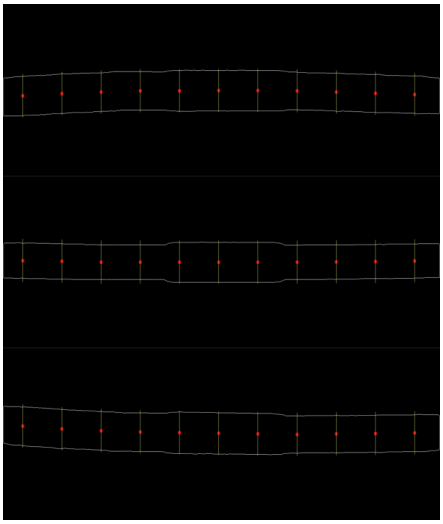

d) Joint sampling point image

Figure 12. Processed image of joint 2

From the axial deviation plots of joints 1 and 2, it can be seen that the three measurements have the same trend of joint

circumference variation, and the overall axial deviation of joint 2 is higher than that of joint 1. The results show that the straightness detection repeatability of the straightness measurement method in this paper is high, and joint 2 has a higher straightness error. It is known from the previous text that the straightness error of joint 1 measured multiple times by the coordinate measuring machine is 7.793 mm, and the straightness error of joint 2 is 10.681 mm. According to the crimping standard, the straightness error of the joint shall not exceed 2% of the tube length, so joint 1 meets the crimping requirement, while joint 2 does not meet the crimping requirement.

Table 3. Experimental data of joint 2 (mm)

Sampling Location	d_i		
	First Sampling	Second Sampling	Third Sampling
20	5.322	5.051	5.457
70	3.887	4.245	4.455
120	4.378	4.577	4.458
170	5.572	5.497	5.191
220	5.639	5.350	5.061
270	4.666	4.909	4.617
320	4.576	4.375	4.542
370	4.118	3.806	4.212
420	4.216	4.563	4.762
470	5.197	5.237	4.872
d_{max}	5.639	5.497	5.457
Straightness error	11.278	10.994	10.914
Mean straightness error	11.062		

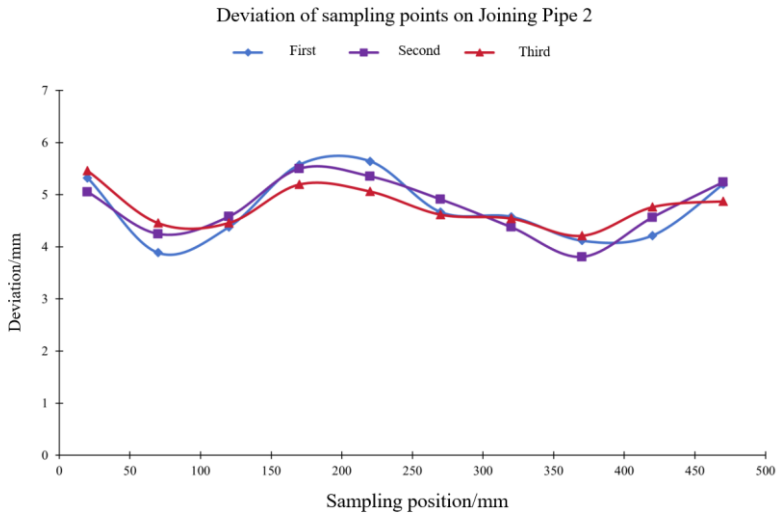

Figure 13. Axial deviation of joint 2

From Table 2 and Table 3, it can be seen that the average straightness error of joint 1 measured multiple times by the straightness measurement method in this paper is 8.075 mm, which is 3.62% different from the measurement result of the coordinate measuring machine, and meets the crimping requirement; the average straightness error of joint 2 is 11.062 mm, which is 3.57% different from the measurement result of the coordinate measuring machine, and does not meet the crimping requirement.

Compared with the measurement results of the measuring instrument, the measurement results of this paper are correct, and the difference between the visual measurement value and the actual measurement value is within 4%, indicating that this method has high measurement accuracy.

CONCLUSION

Aiming at the problems of low detection efficiency and low accuracy of straightness error detection of crimped joints, this paper proposes a machine vision-based straightness error detection technology for joints, which can quickly screen out unqualified crimped joints. This paper has the following characteristics for the straightness measurement of joints:

A modified Grab Cut segmentation method is proposed. The color space of the acquired joint image is converted, and LBP features are extracted. The extracted features are fused and then subjected to principal component analysis, which is suitable for the Grab Cut algorithm. Experiments show that the feature-enhanced Grab Cut segmentation algorithm proposed in this paper can obtain a more clear joint region compared with the traditional Grab Cut segmentation algorithm.

The contour obtained by edge detection based on the above-obtained joint region is more accurate than that obtained by directly performing Canny edge detection on the acquired joint image, which directly affects the accuracy of the straightness error of the joint obtained subsequently.

Based on the three-angle two-dimensional joint axis obtained through the above processing, the corresponding relationship between the two-dimensional image coordinates and the spatial coordinates is used to transform and solve, and then the three-dimensional center coordinates of each cross-section of the joint are obtained. The least squares method is used to fit the evaluation baseline, and the shortest distance of the axial straightness error is searched and compared. Through the comparison test between the visual detection method and the coordinate measuring machine, it is verified that the method in this paper has the advantages of high detection accuracy, good real-time performance, and convenience, and has high practical application value.

At the same time, the straightness measurement method studied in this paper also has some shortcomings. The accuracy of the straightness error in this paper depends on the resolution of the camera used to acquire the joint image. Using a camera with a higher resolution will also increase the cost. The measurement method in this paper requires that the camera be calibrated and the distance between the camera and the joint be fixed. If the length of the joint exceeds the measurement range, it may be necessary to use image stitching or adjust the position of the camera for recalibration.

To address the above shortcomings, image stitching algorithms can be added to the measurement method in the future to further improve the resolution of the acquired images, thereby improving the measurement range and measurement accuracy.

REFERENCES

[1] Jiang H, Zhou W, Lai M, et al. Process defect analysis and visual detection of aluminum/copper cable joints with magnetic pulse crimping. Thin-Walled Structures, 2024: 112110.

[2] Lai M, Wang S, Jiang H, et al. Quality prediction for magnetic pulse crimping cable joints based on 3D vision and ensemble learning. Computers in Industry, 2024, 162: 104137.

[3] Yu L, Li M, Xia X, et al. Rail straightness detection method based on the cooperation of dual laser sensors. Measurement, 2022, 199: 111435.

[4] Zhou Z, Yang H, Liu J. Research on the measurement of the rail straightness based on the outer boundary support point model. Optik, 2020, 223: 165591.

[5] Xiao G, Li Y, Xia Q, et al. Research on the on-line dimensional accuracy measurement method of conical spun workpieces based on machine vision technology. Measurement, 2019, 148: 106881.

[6] Chen B, Mao W, Lou Y, et al. Simultaneous measurement of the straightness error and its position using a modified Wollaston-prism-sensing homodyne interferometer. Measurement Science and Technology, 2020, 31(8): 085004.

[7] Felisiak P, Chorowski M, Poliński J, et al. Measurement of cryogenic valve straightness without accessing valve exterior. Cryogenics, 2024, 140: 103840.

[8] HAO F, SHI J F, MENG C, et al. Measuring straightness errors of slender shafts based on coded references and geometric constraints. The Journal of Engineering, 2020, 2020(6): 221-227.

[9] Lu Y, Duanmu L, Zhai Z J, et al. Application and improvement of Canny edge-detection algorithm for exterior wall hollowing detection using infrared thermal images. Energy and Buildings, 2022, 274: 112421.

[10] Joy Y L, Jerine S. Prediction of skin diseases using grab cut based segmentation with hybrid SCH feature extraction and optimized RBFN algorithm. Biomedical Signal Processing and Control, 2024, 96: 106558.

[11] Koniar D, Volak J, Hargas L, et al. Depth cameras calibration for obstructive sleep apnea diagnostic support//2020 ELEKTRO. IEEE, 2020: 1-6.

[12] Wu M, Zhong Q. Image enhancement algorithm combining histogram equalization and bilateral filtering. Systems and Soft Computing, 2024, 6: 200169.

[13]Kondo Y, Numada M, Yoshida I, et al. Robust filter compatible with Gaussian Filter using L2-Norm. Precision Engineering, 2022, 76: 124-132.

[14] Sahayaraj K K A, Laad A, Mishra A, et al. Optimized Liver Tumor Segmentation: Integrating U-Net with Graph Cut Algorithms//2024 10th International Conference on Communication and Signal Processing (ICCSP). IEEE, 2024: 220-224.

[15] Prusty B R, Bingi K, Gupta N. Review of Gaussian mixture model-based probabilistic load flow calculations//2022 International Conference on Intelligent Controller and Computing for Smart Power (ICICCSP). IEEE, 2022: 01-05.

[16] Chakraborty D, Mills B N, Cheng J, et al. Maximum A-posteriori probability (map) terahertz parameter extraction for pancreatic ductal adenocarcinoma//2022 47th International Conference on Infrared, Millimeter and Terahertz Waves (IRMMW-THz). IEEE, 2022: 1-2.

[17] Han L, Yang T, Pu X, et al. Alzheimer's disease classification using LightGBM and Euclidean distance map//2021 IEEE 5th Advanced Information Technology, Electronic and Automation Control Conference (IAEAC). IEEE, 2021, 5: 1540-1544.

[18] Hu S, Li J, Fan H, et al. Scale and pattern adaptive local binary pattern for texture classification. Expert Systems with Applications, 2024, 240: 122403.

[19] Krishnannair S. Industrial Process Fault Detection Using Singular Spectrum Analysis and Kernel Principal Component Analysis//2020 IEEE Symposium Series on Computational Intelligence (SSCI). IEEE, 2020: 871-875.

[20] Yakoub Z, Amairi M, Chetoui M, et al. Bias Recursive Least Squares Method for Fractional Order System Identification//2022 19th International Multi-Conference on Systems, Signals & Devices (SSD). IEEE, 2022: 1003-1008.